Switchable slow relaxation of magnetization in photochromic dysposium(III) complexes manipulated by dithienylethene ligand

Ming Kong,[a] Xin Feng,[a] Jing Li,[a] Jia Wang,[a] Yi-Quan Zhang,*[b] and You Song*[a]

[a] State Key Laboratory of Coordination Chemistry, School of Chemistry and Chemical Engineering, Collaborative Innovation Center of Advanced Microstructure, Nanjing University, Nanjing 210023, People's Republic of China

[b] Jiangsu Key Laboratory For NSLSCS, School of Physical Science and Technology, Nanjing Normal University, Nanjing 210023, People's Republic of China

* Email: yousong@nju.edu.cn; zhangyiquan@njnu.edu.cn.

Materials and methods

All chemicals and solvents are commercially available and used without further purification. The photochromic ligand of Lo was synthesized according to literature.[S1] Elemental analyses of C, H and N were recorded on a PerkinElmer 240C elemental analyzer. The infrared spectroscopy (IR) was prepared as KBr pellets, and spectra were obtained in the 400−4000 cm^{-1} range using a Vector22 Bruker spectrophotometer. Powder X-ray diffraction (PXRD) patterns were obtained on a D8 ADVANCE X-ray diffractometer with Cu Kα radiation (λ = 1.5405 Å). UV/Vis absorption spectra were recorded using UV 3600 spectrometer. Magnetic susceptibility measurements for polycrystalline samples were performed on a Quantum Design SQUID vibrating sample magnetometer (VSM) in the temperature range from 1.8 to 300 K for direct current (dc). Alternating current (ac) susceptibilities were obtained using an oscillating ac field of 2 Oe and in the frequency range 1-999 Hz. All magnetic data were corrected for the sample holder, the eicosane, and the diamagnetic contribution of the sample.

X-ray Crystallography

The single-crystal X-ray measurements were carried out on a Bruker D8 venture diffractometer fitted with a PHOTON-100 COMS detector with Mo Kα radiation (λ = 0.71073 Å) by using an ω scan mode at 193 K. The diffraction data were treated using SAINT, and all absorption corrections were carried out by using SADABS. All non-hydrogen atoms were labelled by Patterson's method using the SHELXS programs of the SHELXTL package and by subsequent difference Fourier syntheses. The all hydrogens were determined theoretically and refined with isotropic thermal parameters riding on their parents. All non-hydrogen atoms were refined by a full-matrix least-squares technique based on F^2. All calculations were performed by SHELXTL-97.[S2-S4]
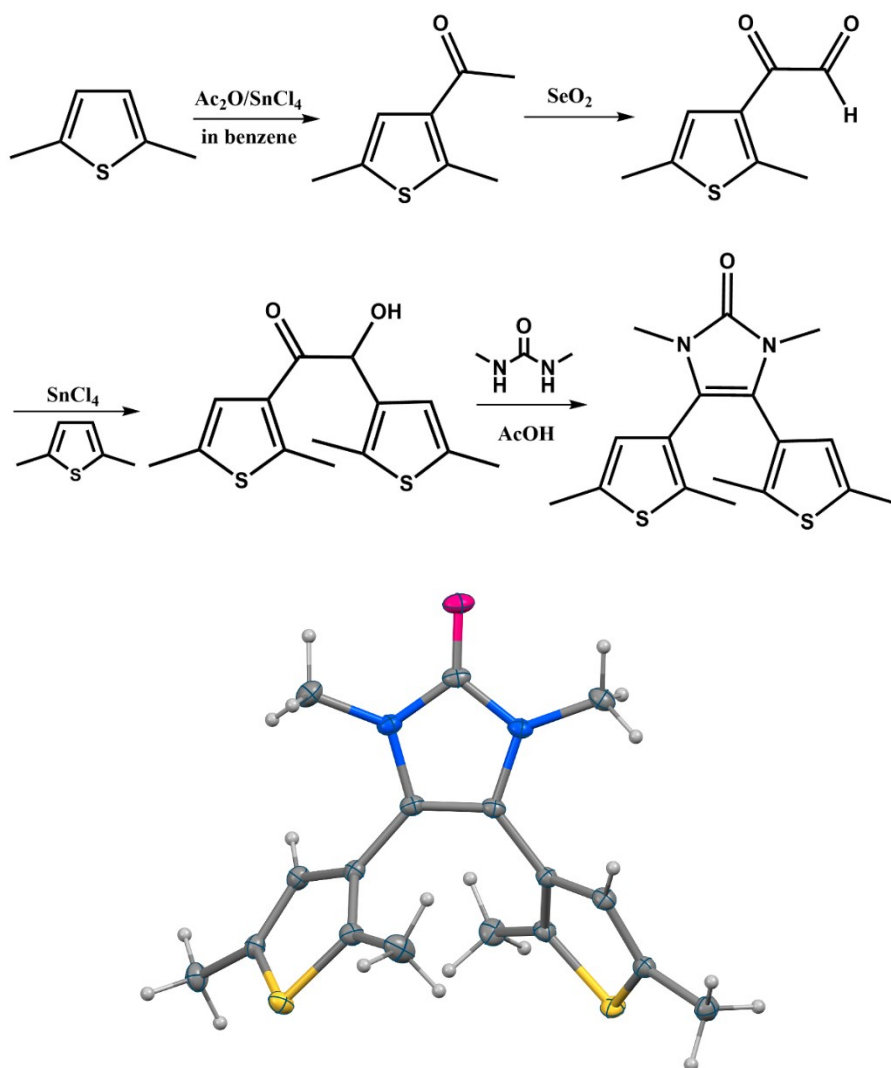
DFT/TD-DFT Calculations

Without any symmetry restraint, time-dependent density functional theory (TD-DFT) and DFT calculations based on the crystal structures from literature[S1] in vacuum were performed to elucidate the electronic structures with the Gaussian 09 software using a B3LYP function. The lowest 100 singlet ground state and singlet-singlet excitation energy levels were calculated with a basis set of 6-31 G* for C H N O S atoms. An analytical frequency confirmed evidence that the calculated species represents a true minimum without imaginary frequencies on the respective potential energy surface.
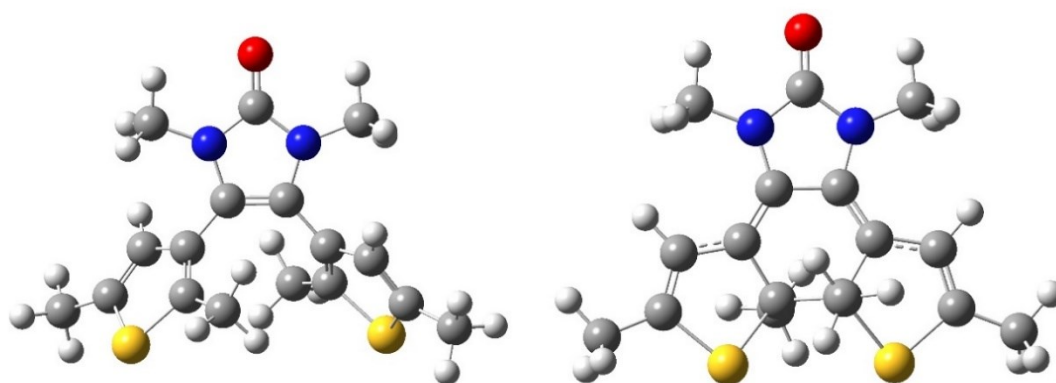
***Ab initio* Calculations**

Complete-active-space self-consistent-field (CASSCF) calculations based on the experimental single crystal X-ray data were performed with the MOLCAS 8.4 program package on individual Dy(III) fragment for each complex. For CASSCF calculations, the basis sets used are atomic natural orbitals from the MOLCAS ANO-RCC library: ANO-RCC-VTZP for Dy(III) ion; VDZP for close O; VDZ for distant atoms. The calculations employed the second order Douglas-Kroll-Hess Hamiltonian, where scar relativistic contractions were taken into account in the basis set and the spin-orbit coupling were handled separately in the restricted active space state (RASSI-SO) procedure. The active electrons in seven active spaces contain all *f* electrons CAS (9 in 7) for each Dy(III) fragment. The

maximum number of spin-free states that are possible with our hardware include all 21 sextets, 128 from 224 quadruplets, and 130 from 490 doublets for Dy(III) fragment.[S5]
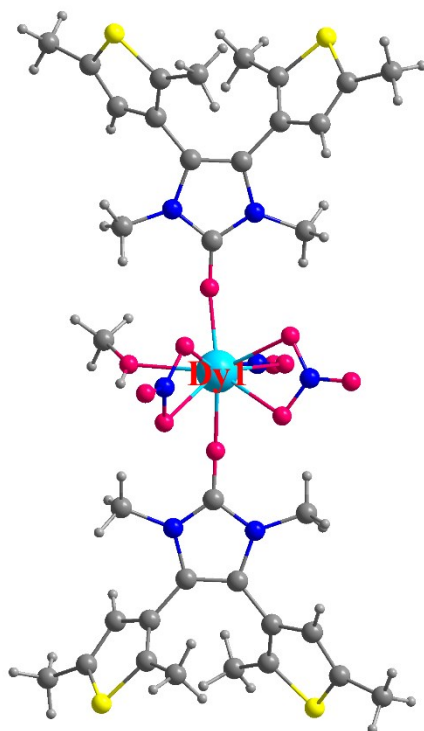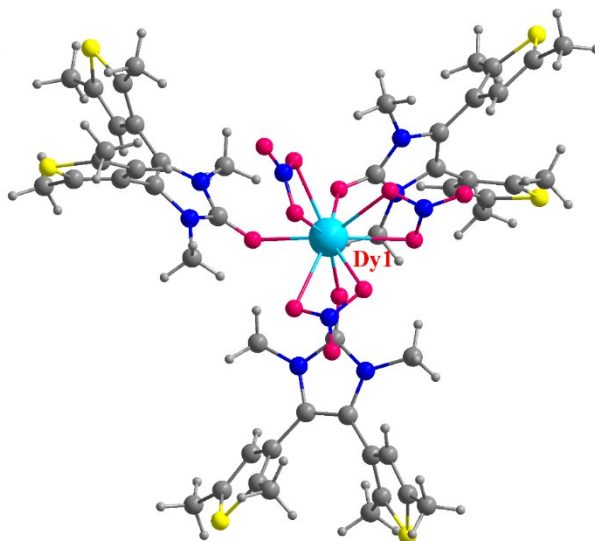
Scheme S1 Synthesis route of Lo.

Fig. S1 Crystal structures for Lo with 30% probability. Color code: O, red; N, blue; C, gray; S, yellow.


Fig. S2 The DFT and TD-DFT calculation models of ring-open and ring-close ligands based on the crystal structures.

Fig. S3 *ab initio* calculated Dy(III) fragment of **1-o**; H atoms are omitted for clarity. Color code: Dy, light-blue; O, red; N, blue; C, gray; S, yellow.

Fig. S4 The *ab initio* calculated Dy(III) fragment of **2-o**; H atoms are omitted for clarity. Color code: Dy, light-blue; O, red; N, blue; C, gray; S, yellow.
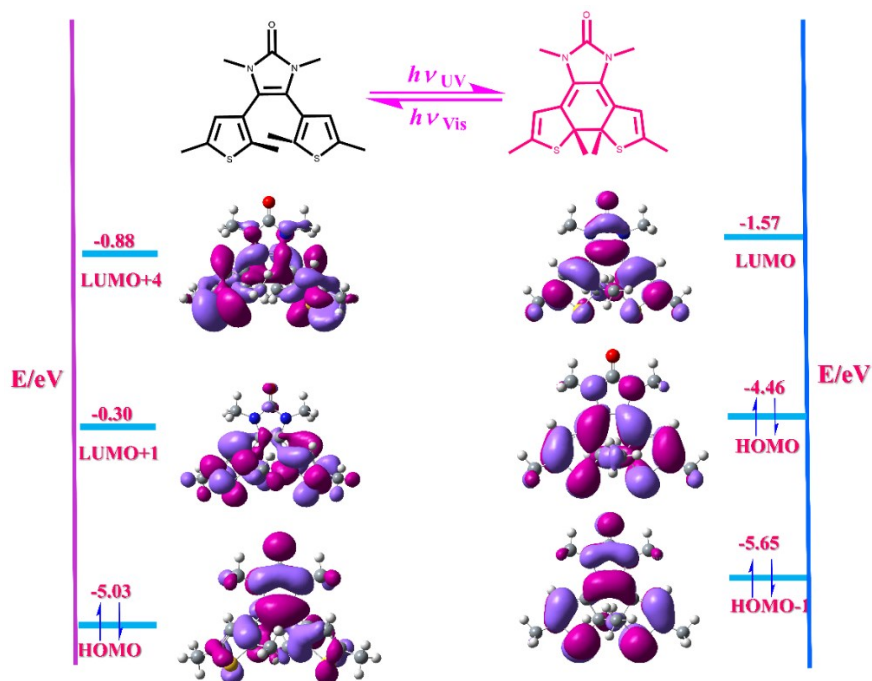
Fig. S5 The calculated transition molecular orbital diagrams for the DAE ligand of Lo and Lc.

Table S1 Selected experimental and calculated optical data for Lo and Lc

compound	OI[a]	ΔE (eV)[b]	Cal. λ_{max} (nm) [c]	Obs. λ_{max} (nm) [d]	f [e]	character
Lo	H → L+1	4.0957	303	280	0.0460	n→π*/π→π*
	H → L+4	5.2015	238	235	0.1224	n→π*
Lc	H-1→ L	3.5669	348	315	0.1522	n→π*/π→π*
	H→ L	2.5051	495	475	0.2186	π→π*

[a] Orbitals involved in the excitations, [b] Excitation energies (eV), [c] Calculated peak position of the longest absorption band, [d] Observed peak position of the absorption band, [e] Oscillator Strengths, H represents HOMO, L represents LUMO.
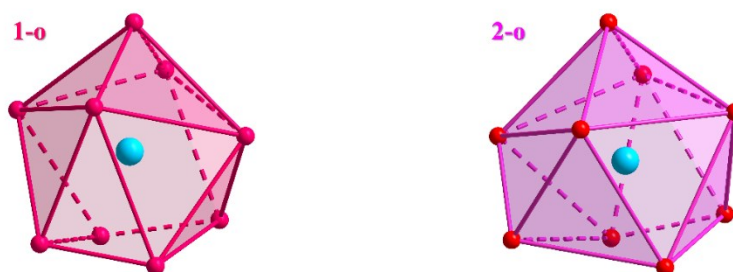
Fig. S6 The coordination geometries of metal centers in complexes **1-o** and **2-o**. Color code: Dy, light-blue; O, red.
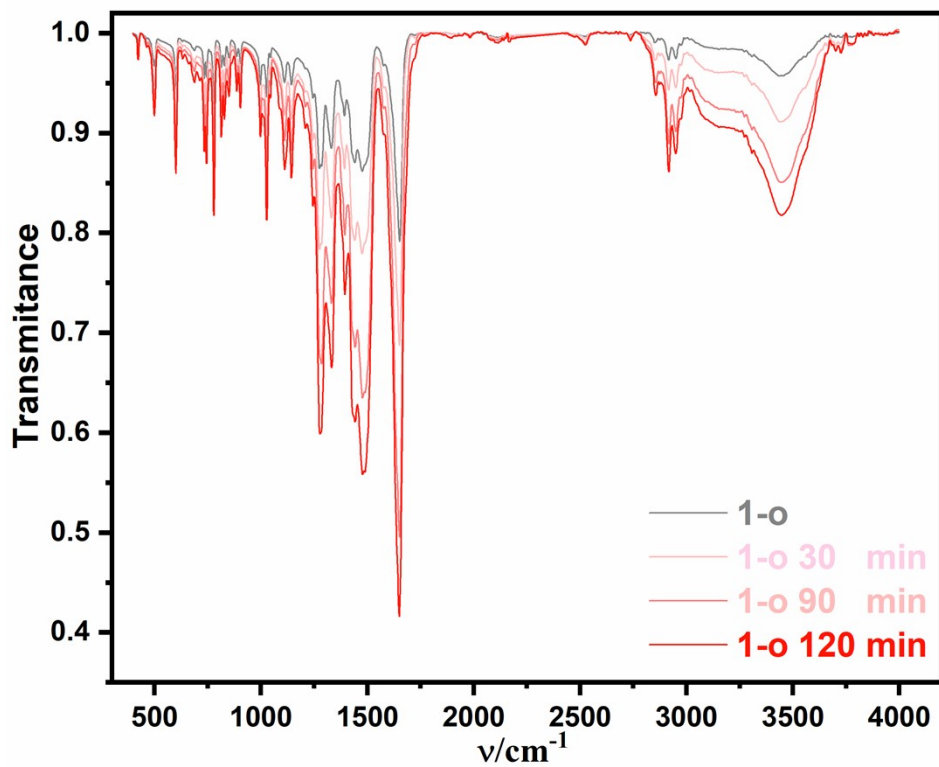
Fig. S7 Changes in IR spectra for a powdered sample of **1-o** upon irradiating with 254 nm light.
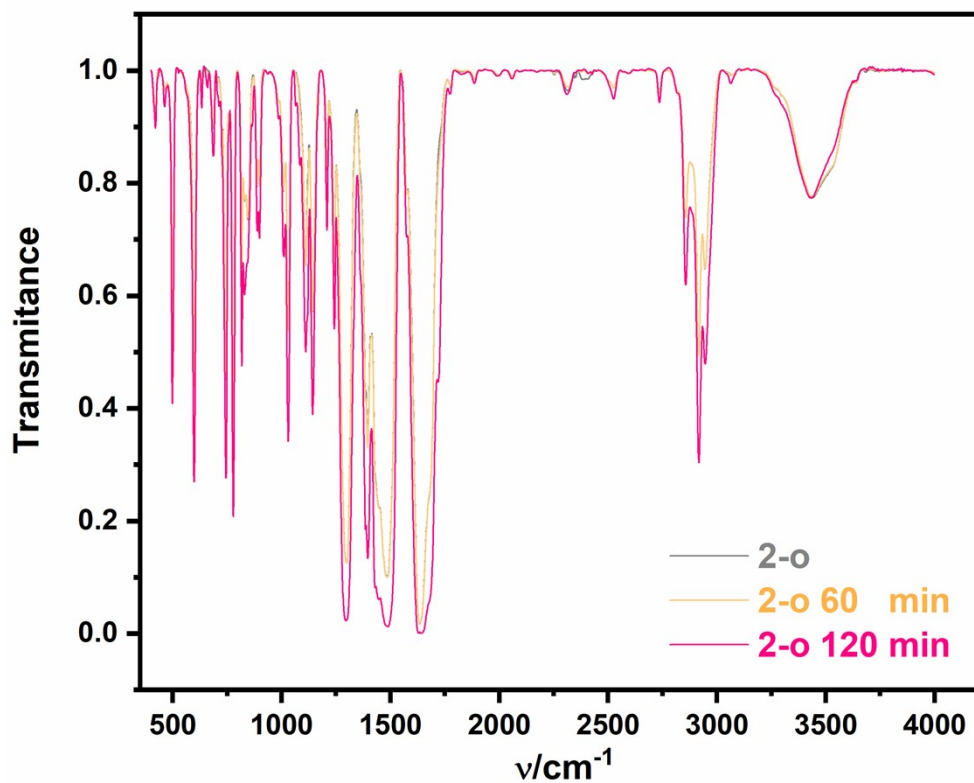

Fig. S8 Changes in IR spectra for a powdered sample of **2-o** upon irradiating with 254 nm light.

Table S2 Crystallographic refinement parameters for **1-o**, **2-o** and **Lo**.

	1-o	2-o	Lo
Empirical formula	$C_{35}H_{44}DyN_7O_{12}S_4$	$C_{51}H_{60}DyN_9O_{12}S_6$	$C_{17}H_{20}N_2OS_2$
Formula weight	1045.51	1345.94	332.47
Crystal system	Monoclinic	Triclinic	Triclinic
space group	$P2_1/n$	$P\bar{1}$	$P\bar{1}$
T / K	193	193	193
a (Å)	7.7601(2)	8.9475(6)	7.4367(7)
b (Å)	29.8742(10)	18.8073(12)	8.9281(3)
c (Å)	18.9588(6)	21.2856(14)	13.7147(6)
α (°)	90	77.660(3)	97.790(3)
β (°)	94.4050(10)	89.468(3)	101.096(10)
γ (°)	90	87.737(3)	108.161(2)
V (Å^3)	4382.2(2)	3496.4(4)	830.18(13)
Z	4	2	2
F (000)	2116.0	1374	352.0
GOF on F^2	1.107	1.062	1.124
R_1/WR_2 [$I>2\sigma(I)$]	0.0659 / 0.1609	0.0817 / 0.2160	0.0490 / 0.1373
R_1/WR_2 [all data]	0.0863 / 0.1687	0.0994 / 0.2276	0.0495 / 0.1377
CCDC No.	2023573	2023574	2023575

Table S3 Selected bond lengths (Å) for **1-o** and **2-o**

1-o / Å		2-o / Å	
Dy(1)-O(1)	2.241(9)	Dy(1)-O(1)	2.294(5)
Dy(1)-O(2)	2.226(8)	Dy(1)-O(2)	2.273(6)
Dy(1)-O(3)	2.416(10)	Dy(1)-O(3)	2.320(6)
Dy(1)-O(5)	2.441(9)	Dy(1)-O(4)	2.485(7)
Dy(1)-O(6)	2.407(9)	Dy(1)-O(5)	2.445(7)
Dy(1)-O(8)	2.457(11)	Dy(1)-O(7)	2.455(7)
Dy(1)-O(9)	2.423(10)	Dy(1)-O(8)	2.495(6)
Dy(1)-O(12)	2.455(10)	Dy(1)-O(10)	2.456(6)
		Dy(1)-O(11)	2.502(7)

**Table S4** Selected bond angles (°) for **1-o** and **2-o**.

1-o / °		2-o / °	
O(2)-Dy(1)-O(1)	153.3(4)	O(2)-Dy(1)-O(1)	83.8(3)
O(2)-Dy(1)-O(6)	85.5(3)	O(2)-Dy(1)-O(3)	84.3(3)
O(1)-Dy(1)-O(6)	82.1(3)	O(1)-Dy(1)-O(3)	83.5(3)
O(2)-Dy(1)-O(3)	79.2(4)	O(2)-Dy(1)-O(5)	146.5(3)
O(1)-Dy(1)-O(3)	88.3(3)	O(1)-Dy(1)-O(5)	85.4(3)
O(6)-Dy(1)-O(3)	123.8(3)	O(3)-Dy(1)-O(5)	125.7(3)
O(2)-Dy(1)-O(9)	126.7(4)	O(2)-Dy(1)-O(10)	85.9(3)
O(1)-Dy(1)-O(9)	74.7(3)	O(1)-Dy(1)-O(10)	126.2(3)
O(6)-Dy(1)-O(9)	82.0(3)	O(3)-Dy(1)-O(10)	147.4(3)

| O(3)-Dy(1)-O(9)	147.3(4)	O(5)-Dy(1)-O(10)	75.3(3)
O(2)-Dy(1)-O(5)	79.5(4)	O(2)-Dy(1)-O(7)	125.9(3)
O(1)-Dy(1)-O(5)	74.2(3)	O(1)-Dy(1)-O(7)	147.2(3)
O(6)-Dy(1)-O(5)	52.4(3)	O(3)-Dy(1)-O(7)	85.8(3)
O(3)-Dy(1)-O(5)	71.7(4)	O(5)-Dy(1)-O(7)	76.1(3)
O(9)-Dy(1)-O(5)	127.3(3)	O(10)-Dy(1)-O(7)	75.0(3)
O(2)-Dy(1)-O(12)	77.8(3)	O(2)-Dy(1)-O(4)	150.9(3)
O(1)-Dy(1)-O(12)	123.7(3)	O(1)-Dy(1)-O(4)	74.5(3)
O(6)-Dy(1)-O(12)	146.8(3)	O(3)-Dy(1)-O(4)	74.4(3)
O(3)-Dy(1)-O(12)	81.2(4)	O(5)-Dy(1)-O(4)	51.4(3)
O(9)-Dy(1)-O(12)	85.3(4)	O(10)-Dy(1)-O(4)	122.5(3)
O(5)-Dy(1)-O(12)	147.3(3)	O(7)-Dy(1)-O(4)	72.8(3)
O(2)-Dy(1)-O(8)	75.3(4)	O(2)-Dy(1)-O(8)	74.3(3)
O(1)-Dy(1)-O(8)	122.8(3)	O(1)-Dy(1)-O(8)	150.7(3)
O(6)-Dy(1)-O(8)	73.5(3)	O(3)-Dy(1)-O(8)	75.5(2)
O(3)-Dy(1)-O(8)	147.8(3)	O(5)-Dy(1)-O(8)	123.5(3)
O(9)-Dy(1)-O(8)	51.5(3)	O(10)-Dy(1)-O(8)	72.0(3)
O(5)-Dy(1)-O(8)	121.3(3)	O(7)-Dy(1)-O(8)	51.7(3)
O(12)-Dy(1)-O(8)	74.6(3)	O(4)-Dy(1)-O(8)	117.7(3)
O(2)-Dy(1)-O(11)	122.6(3)	O(2)-Dy(1)-O(11)	74.0(3)
O(1)-Dy(1)-O(11)	73.4(3)	O(1)-Dy(1)-O(11)	74.9(3)
O(6)-Dy(1)-O(11)	151.8(3)	O(3)-Dy(1)-O(11)	150.7(3)
O(3)-Dy(1)-O(11)	69.9(4)	O(5)-Dy(1)-O(11)	72.6(3)
O(9)-Dy(1)-O(11)	78.4(4)	O(10)-Dy(1)-O(11)	51.5(3)
O(5)-Dy(1)-O(11)	129.7(3)	O(7)-Dy(1)-O(11)	122.9(3)
O(12)-Dy(1)-O(11)	51.1(3)	O(4)-Dy(1)-O(11)	117.1(3)
O(8)-Dy(1)-O(11)	108.5(3)	O(8)-Dy(1)-O(11)	115.8(2)

Table S5 The evaluated local geometry analysis for **1-o** and **2-o** by SHAPE software.

| shape	symmetry	distortion (τ)	
		1-o	**2-o**
Capped cube J8	C_{4v}	8.537	10.376
Spherical-relaxed capped cube	C_{4v}	7.105	9.291
Capped square antiprism J10	C_{4v}	3.446	3.357
Spherical capped square antiprism	C_{4v}	**2.665**	**2.433**
Tricapped trigonal prism J51	D_{3h}	3.331	2.685
Spherical tricapped trigonal prism	D_{3h}	2.784	2.066
Hula-hoop	C_{2v}	8.934	-
Tridiminished icosahedron J63	C_{3v}	-	10.975
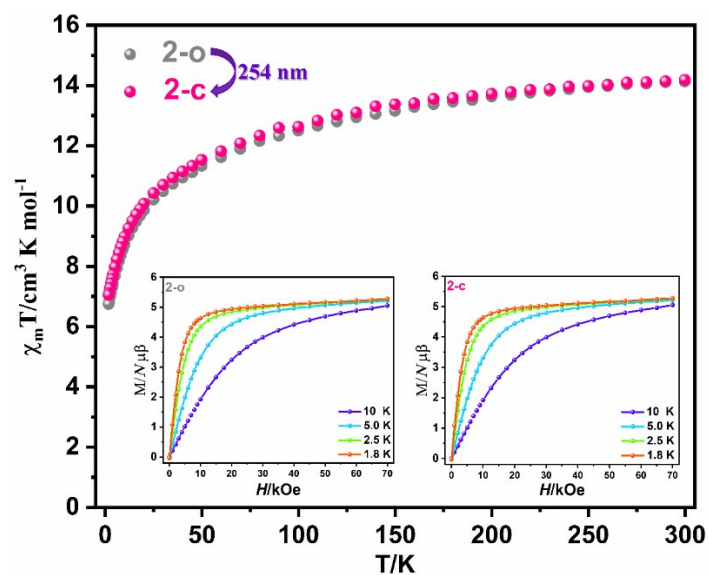
Fig. S9 The variable-temperature magnetic susceptibilities of **2-o** and **2-c** under an external field of 1 kOe in the temperature range of 1.8-300 K. The insets represent field-dependent magnetization at 1.8, 2.5, 5.0 and 10 K.
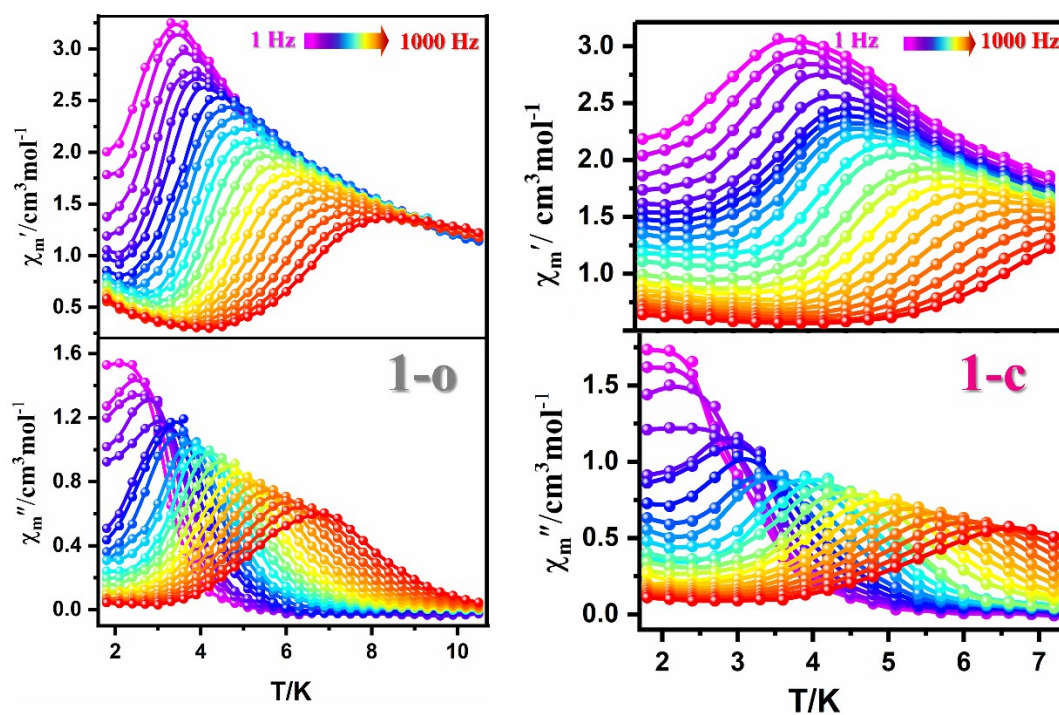
Fig. S10 Temperature dependence of in-phase (χ') and out-of-phase (χ'') ac magnetic susceptibility of **1-o** and **1-c** in 800 Oe dc field.
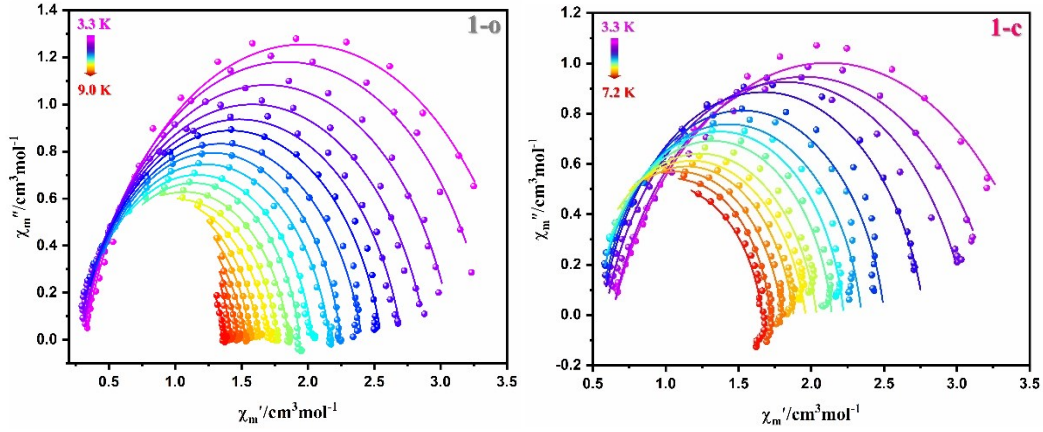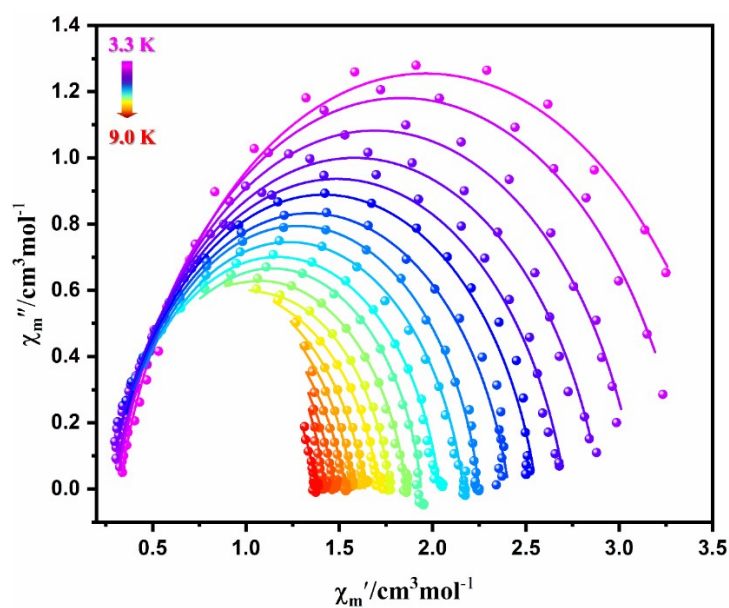
Fig. S11 The Cole-Cole fitted data for **1-o** and **1-c** under the optimal field (800 (**1-o**), and 800 (**1-c**) Oe) by generalized Debye model (the solid lines represent the best results).

Table S6 Fitting results of the Cole-Cole plots for **1-o** with a generalized Debye model under 800 Oe dc field.

T / K	χ_S / cm^3· mol^{-1}	χ_T / cm^3 · mol^{-1}	τ	α
3.29997	0.32099	3.60939	0.03053	0.16399
3.59999	0.30486	3.36056	0.0172	0.15603
3.89907	0.28964	3.09404	0.00957	0.15689
4.20013	0.26604	2.89751	0.00556	0.16657
4.50012	0.26265	2.71141	0.00338	0.16272
4.79991	0.27842	2.5555	0.00215	0.14977
5.10012	0.27844	2.40822	0.00139	0.14856
5.4	0.30813	2.24869	9.02078E-4	0.11932
5.70017	0.29621	2.16482	6.28299E-4	0.13543
6.0001	0.29682	2.03682	4.33739E-4	0.1297
6.30007	0.34236	1.93887	3.19964E-4	0.10704
6.6002	0.29383	1.8596	2.23869E-4	0.13204
6.89221	0.31446	1.77106	1.66325E-4	0.12213
7.20078	0.18686	1.71536	1.07264E-4	0.16159
7.50005	0.06838	1.63882	7.03842E-5	0.16518
7.80005	0.10965	1.57068	5.68541E-5	0.1375
8.09993	2.04331E-9	1.53423	3.68288E-5	0.17733
8.40005	3.10129E-9	1.47456	2.90676E-5	0.15132
8.70009	5.05249E-9	1.42	2.48403E-5	0.09857
9.00005	7.265E-9	1.37671	1.75396E-5	0.1496

Table S7 Fitting results of the Cole-Cole plots for **1-c** with a generalized Debye model under 800 Oe dc field.

T / K	χ_S / cm^3· mol^{-1}	χ_T / cm^3 · mol^{-1}	τ	α
3.3	0.63173	3.59347	0.02312	0.23824
3.60001	0.63392	3.27415	0.0148	0.20276
3.90006	0.58252	3.07316	0.00877	0.18049
4.20005	0.56124	2.77652	0.00472	0.13451
4.50005	0.55265	2.50144	0.0028	0.1075
4.79997	0.52611	2.3452	0.00183	0.10798
5.10001	0.52444	2.2222	0.0012	0.0888
5.40014	0.50557	2.14091	8.38716E-4	0.0982
5.70015	0.43715	2.0371	5.59414E-4	0.13297
6.00001	0.40256	1.96094	3.91365E-4	0.14502
6.30353	0.41831	1.87722	2.83971E-4	0.12671
6.59998	0.38623	1.79875	2.01966E-4	0.12919
6.89995	0.45825	1.71875	1.59272E-4	0.09528
7.20002	0.42102	1.66147	1.17776E-4	0.12493

Fig. S12 The Cole-Cole fitted data for **1-o** in 800 Oe dc field by generalized Debye model (the solid lines represent the best results).
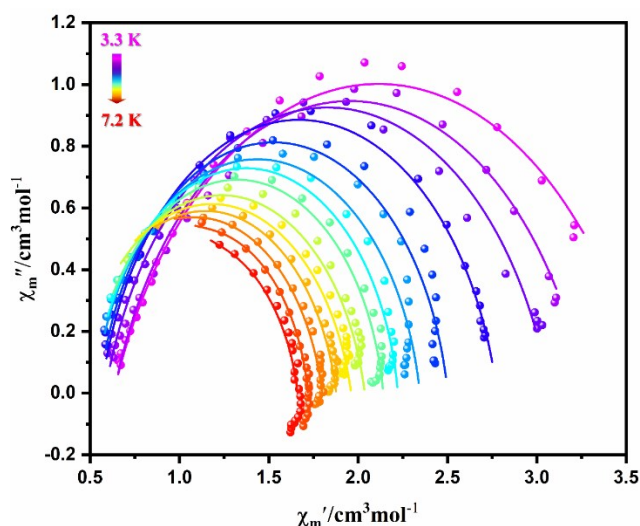
Fig. S13 The Cole-Cole fitted data for **1-c** in 800 Oe dc field by generalized Debye model (the solid lines represent the best results).

Table S8 The calculated energy levels (cm^{-1}), g (g_x, g_y, g_z) tensors and m_J values of the minimum KDs of Dy(III) motifs in complex **1-o** and **2-o**.

		1-o					2-o		
KDs	E / cm^{-1}		g	m_J	KDs	E / cm^{-1}		g	m_J
1	0.0	g_x	0.054	±15/2	1	0.0	g_x	2.586	mixed states
		g_y	0.082				g_y	4.586	
		g_z	19.777				g_z	11.761	
2	105.6 (152.1 K)	g_x	0.512	±13/2	2	9.1 (13.1K)	g_x	2.375	mixed states
		g_y	0.700				g_y	3.506	
		g_z	16.680				g_z	11.364	
3	224.5	g_x	3.036	±11/2	3	34.6	g_x	6.597	mixed states
		g_y	5.902				g_y	5.619	
		g_z	11.210				g_z	4.112	
4	284.8	g_x	6.893	±3/2	4	94.9	g_x	5.069	mixed states
		g_y	6.359				g_y	6.180	
		g_z	2.747				g_z	7.765	
5	358.9	g_x	1.519	±1/2	5	127.0	g_x	0.171	mixed states
		g_y	5.650				g_y	1.932	
		g_z	12.499				g_z	10.781	
6	404.2	g_x	1.780	±9/2	6	155.9	g_x	11.528	mixed states
		g_y	5.047				g_y	6.013	
		g_z	9.121				g_z	0.020	
7	438.7	g_x	1.465	±7/2	7	184.2	g_x	2.114	mixed states
		g_y	3.705				g_y	6.354	
		g_z	13.494				g_z	11.809	
8	514.9	g_x	0.450	±5/2	8	206.6	g_x	0.276	mixed states
		g_y	0.707				g_y	0.566	
		g_z	18.224				g_z	17.210	

Table S9 Wave functions with definite projection of the total moment | m_J > for the lowest two KDs for complexes **1-o** and **2-o**.

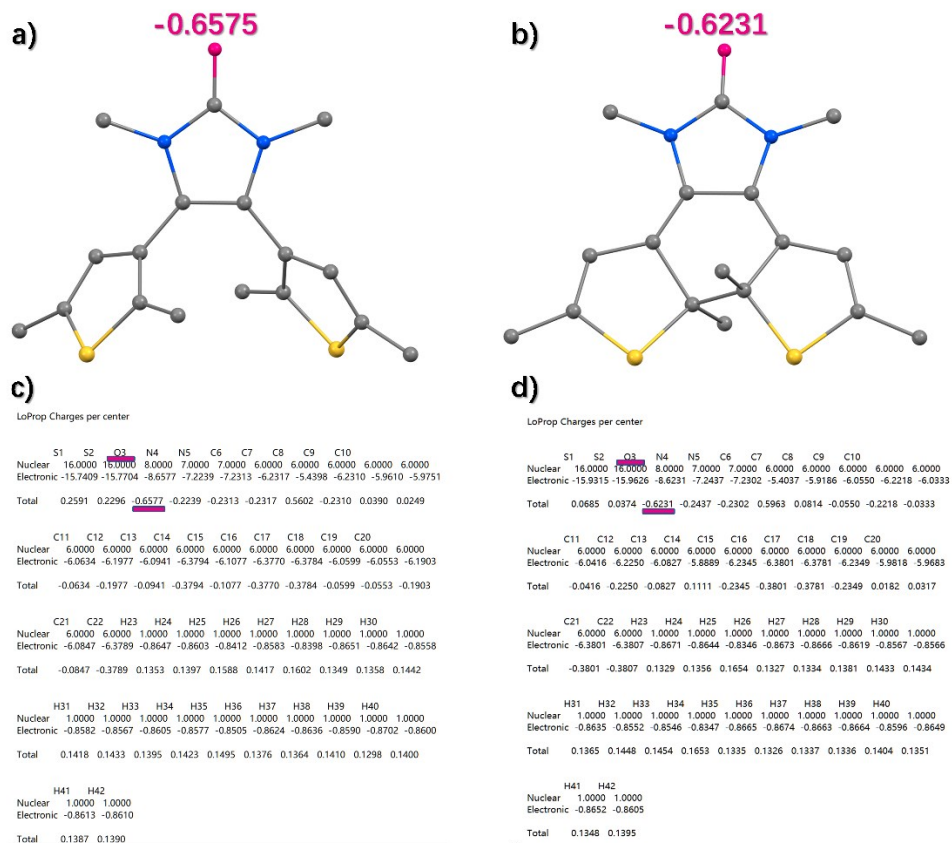|	E	wave functions
1-o	0.0	98.3%|±15/2>
	105.6	94.3%|±13/2>
2-o	0.0	30.6%|±7/2>+29.7%|±11/2>+23.5%|±15/2>+6.7%|±5/2>
	9.1	26.6%|±9/2>+18.9%|±5/2>+14.8%|±3/2>+13.9%|±1/2>+11.1%|±11/2>
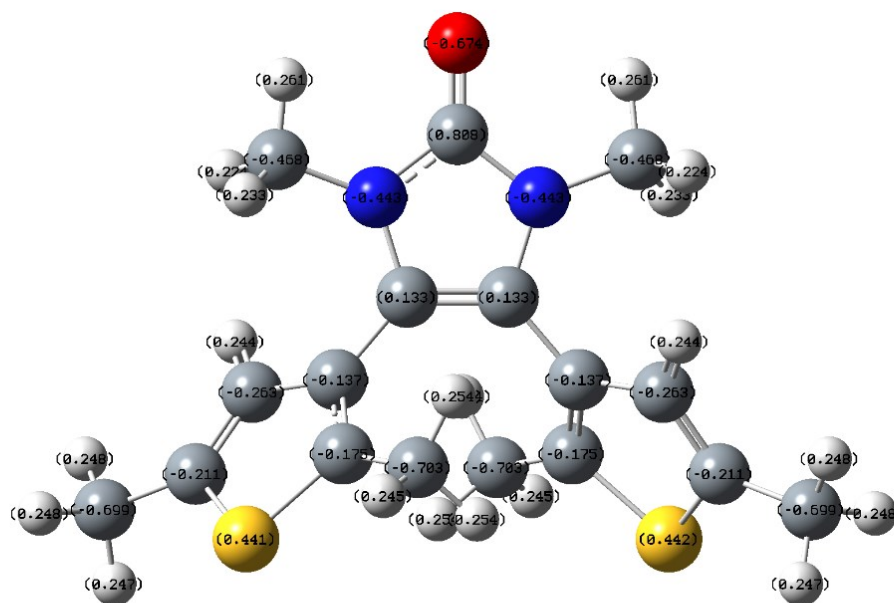
Fig. S14 The NBO charges analysis of the ring-open (Lo) ligands by DFT calculation.
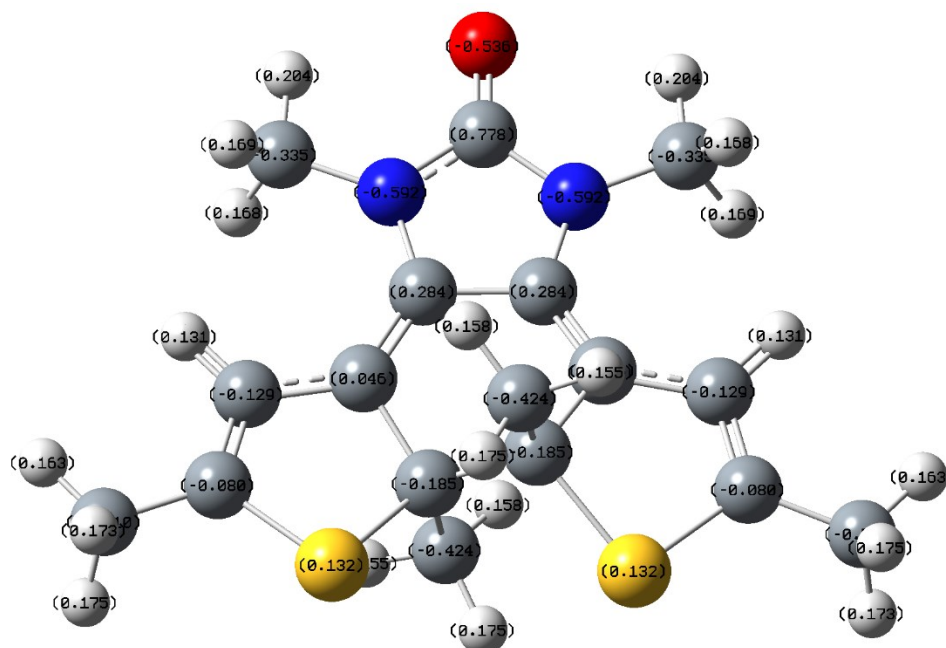
Fig. S15 The NBO charges analysis of the ring-close (Lc) ligands by DFT calculation.

Fig. S16 The LoProp charges analysis of the ring-open (Lo, a and c) and ring-close (Lc, b and d) ligands by RASSCF calculations.
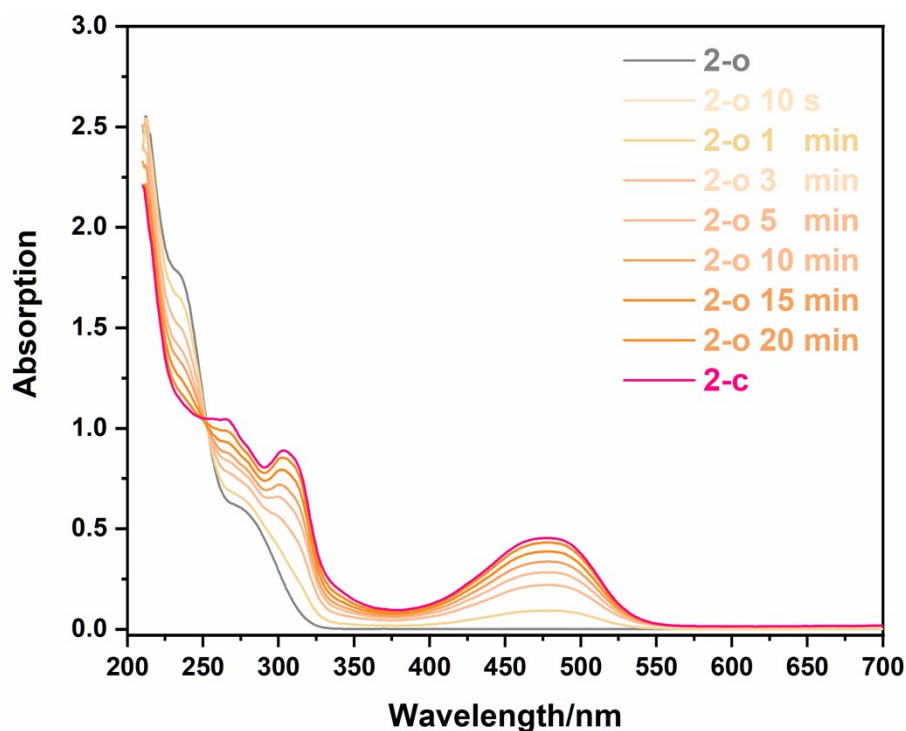
Fig. S17 Changes in the UV/Vis absorption spectra of **2-o** in methanol solution (1.0×10^{-5} M) as irradiated with 254 nm light.
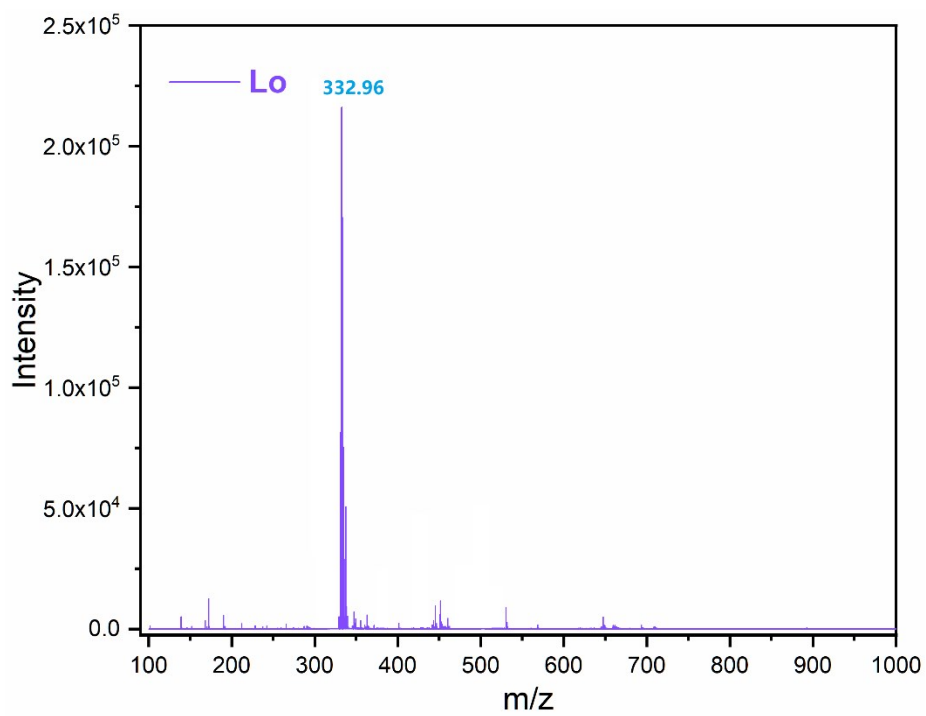
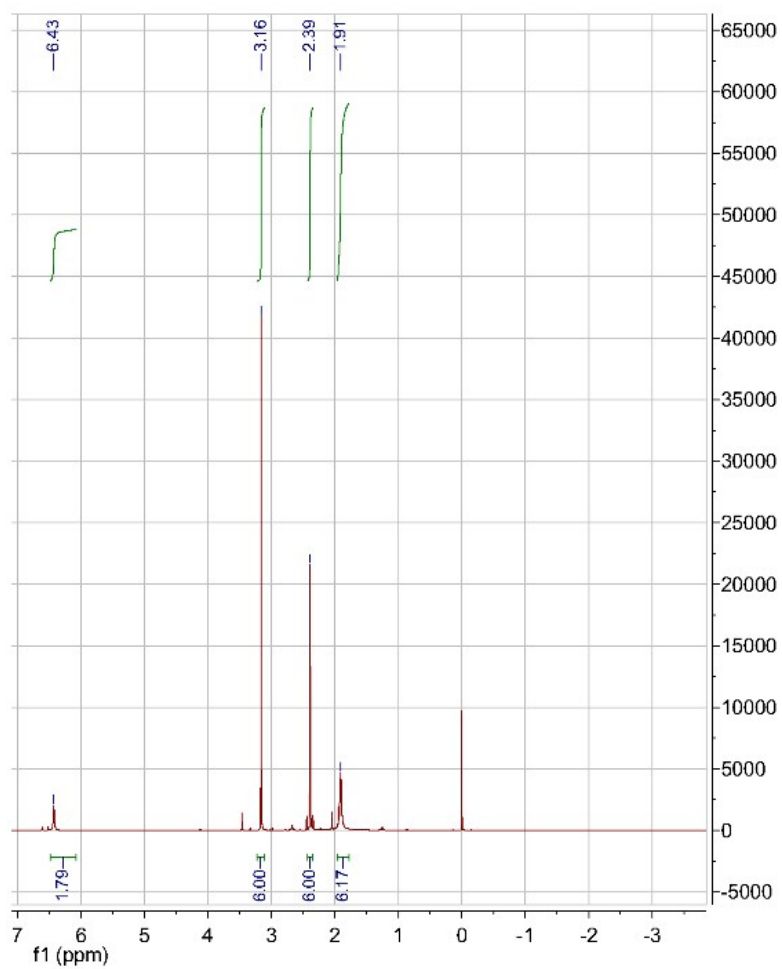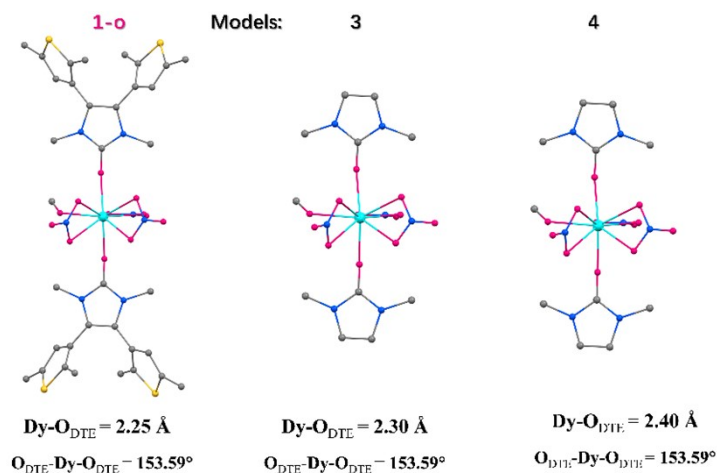**Fig. S18** MALDI-TOF-MS of Lo.

Fig. S19 ^{1}H NMR spectrum of Lo.

Fig. S20 Simplified model complexes of **3** and **4** based on Lc and 1-o with different Dy-O$_{DTE}$ bond distances.

Table S10 The calculated energy levels (cm^{-1}), g (g_x, g_y, g_z) tensors and m_J values of the minimum KDs of Dy(III) motifs in model complexes of **3** and **4**.

3				4			
KDs	E/cm^{-1}	g		m_J	KDs	E/cm^{-1}	g		m_J
1	0.0	g_x 0.27 g_y 0.42 g_z 19.51	mixed states	1	0.0	g_x 0.43 g_y 4.21 g_z 14.88	mixed states
2	45.63	g_x 1.57 g_y 2.16 g_z 15.03	mixed states	2	10.34	g_x 0.11 g_y 3.36 g_z 15.32	mixed states
3	95.73	g_x 2.56 g_y 4.48 g_z 10.61	mixed states	3	62.94	g_x 2.60 g_y 3.24 g_z 14.05	mixed states
4	113.53	g_x 1.12 g_y 1.51 g_z 11.43	mixed states	4	84.94	g_x 1.05 g_y 2.38 g_z 15.13	mixed states
5	174.35	g_x 2.90 g_y 4.28 g_z 9.57	mixed states	5	121.94	g_x 0.24 g_y 3.90 g_z 10.32	mixed states
6	221.84	g_x 0.43 g_y 1.45 g_z 14.24	mixed states	6	144.81	g_x 0.68 g_y 3.11 g_z 10.83	mixed states
7	251.28	g_x 1.01 g_y 3.53 g_z 6.47	mixed states	7	177.08	g_x 0.14 g_y 3.19 g_z 9.34	mixed states
8	278.15	g_x 10.94 g_y 8.47 g_z 2.38	mixed states	8	195.15	g_x 1.66 g_y 6.28 g_z 13.29	mixed states

REFERENCES

S1 B. M. Neilson, V. M. Lynch and C. W. Bielawski, *Angew. Chem. Int. Ed.*, 2011, **50**, 10322-10326.

S2 SAINT-Plus, version 6.02; Bruker analytical X-ray system: Madison, WI, 1999.

S3 G. M. Sheldrick, SADABS an empirical absorption correction program; Bruker Analytical X-ray Systems: Madison, WI, 1996.

S4 G. M. Sheldrick, *Acta Crystallogr., Sect. A: Found. Crystallogr.*, 2008, **A64**, 112.

S5 (a) F. Aquilante, J. Autschbach, R. K. Carlson, L. F. Chibotaru, M. G. Delcey, L. De Vico, I. F. Galván, N. Ferré, L. M. Frutos, L. Gagliardi, M. Garavelli, A. Giussani, C. E. Hoyer, G. Li Manni, H. Lischka, D. Ma, P. Å. Malmqvist, T. Müller, A. Nenov, M. Olivucci, T. B. Pedersen, D. Peng, F. Plasser, B. Pritchard, M. Reiher, I. Rivalta, I. Schapiro, J. Segarra-Martí, M. Stenrup, D. G. Truhlar, L. Ungur, A. Valentini, S. Vancoillie, V. Veryazov, V. P. Vysotskiy, O. Weingart, F. Zapata, and R. Lindh, *J. Comput. Chem.*, 2016, **37**, 506. (b) L. F. Chibotaru, *Struc. Bonding (Berlin, Ger.)*, 2014, **164**, 185. (c) U. Liviu and L. F. Chibotaru, *Inorg. Chem.*, 2016, **55**, 10043. (d) J. J. Baldoví, Y. Duan, R. Morales, A. Gaita-Ariño, E. Ruiz and E. Coronado, *Chem. Eur. J.*, 2016, **22**, 13532. (e) U. Liviu and L. F. Chibotaru, *Phys. Chem. Chem. Phys.*, 2011, **13**, 20086. (f) L. F. Chibotaru and L. Ungur, *J. Chem. Phys.*, 2012, **137**, 064112.